Photofragment Spectroscopy of π Complexes: Au$^+$(C$_2$H$_4$) and Pt$^+$(C$_2$H$_4$)

Kay L. Stringer, Murat Citir, and Ricardo B. Metz*
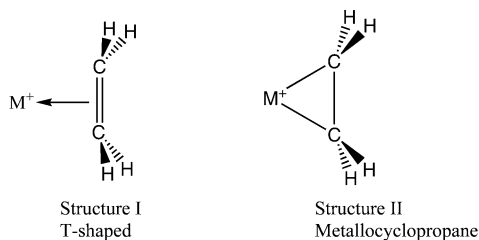
Department of Chemistry, University of Massachusetts−Amherst, Amherst, Massachusetts 01003

Received: May 19, 2004

Photodissociation spectra of the classic π complexes Au$^+$(C$_2$H$_4$) and Pt$^+$(C$_2$H$_4$) in the gas phase are reported, providing upper limits to metal−ligand bond strengths of 28 800 cm^{-1} (344 kJ mol^{-1}) and 19 200 cm^{-1} (230 kJ mol^{-1}), respectively. The spectrum of Au$^+$(C$_2$H$_4$) features an extended progression in the metal−ligand stretch with a frequency of 176 cm^{-1}, which drops to 160 cm^{-1} in Au$^+$(C$_2$D$_4$). Hybrid density functional theory (DFT) calculations at the B3LYP level indicate that both complexes adopt a metallocyclopropane structure. The effect of basis set size and flexibility on the metal−ligand dissociation energy is explored. In addition, excited electronic states of both complexes have been investigated by using TD-DFT calculations.

Introduction

In 1827, Zeise synthesized the first known complex containing a π-bound ligand, K[PtCl$_3$(C$_2$H$_4$)] (Zeise's salt).[1,2] Since this scientific milestone, π complexes have become increasingly important as reagents in chemical synthesis and in industrial processes, primarily due to the significant role they play in various bond activation processes and in catalysis.[3] The bonding in this complex can be described by the Dewar−Chatt−Duncanson model.[4,5] The Pt atom (a σ acceptor) is weakly bound to both carbons of ethylene (a π donor) with the four C−H bonds bending away from the metal, allowing better overlap of the Pt with the π electrons of ethylene. In addition, because Pt(II) is only weakly π basic, metal−ligand σ bonding predominates with minimal π back-donation. So, the C−C bond resembles the free alkene and the complex is T-shaped (structure I). However, in complexes containing the more strongly π basic

Structure I
T-shaped

Structure II
Metallocyclopropane

Pt(0), there is significant π back-donation into the C−C antibonding orbital. This leads toward a metallocyclopropane type structure (structure II) in which the C−C bond lengthens and is reduced to almost a single bond.

The possibility of such organometallic complexes exhibiting different chemical structures has prompted a number of experimental studies[6−10] and reviews[11,12] in an effort to clarify the effects of relativistic contributions and periodicity on such systems. In ab initio studies by Sodupe et al. on complexes of isolated first row transition metal ions with acetylene and ethylene, Sc$^+$ and Ti$^+$ were found to form a three-membered ring (metallocyclopropane), while V$^+$ through Cu$^+$ prefer to form an electrostatic complex with ethylene.[13,14] Although their

* To whom correspondence should be addressed. E-mail: rbmetz@chemistry.umass.edu.

computed binding energies generally agreed with experiment, there were a few discrepancies for the later transition metals. Their conclusions contradict the traditional view that transition metals which are good π donors opt for the metallocyclopropane structure, whereas weaker π donors lead to T-shaped structures. In addition, calculations by Schröder et al.[15,16] predict that Au$^+$ binds to ethylene much more strongly than any other transition metal. This is surprising, as its d^{10} electron configuration would suggest that Au$^+$ would bind less strongly than metals with a partially filled d orbital, such as Pt$^+$. This implies a more complicated explanation for the bonding in M$^+$(C$_2$H$_4$) complexes.

Gas-phase techniques are especially appealing as methods for studying metal−ligand interactions as they avoid many of the interferences and complicating effects that can occur in the condensed phase due to solvation, additional ligands, or counterions.[17−20] An added advantage is that the results can be directly compared to those obtained by theoretical methods. Here, we report an experimental study of the electronic spectroscopy and photodissociation dynamics of Au$^+$ and Pt$^+$ complexes with ethylene. We also present the results of calculations on the ground and excited electronic states of the complexes which aid in interpreting the experiments.

Experimental Approach

The electronic spectroscopy of Au$^+$(C$_2$H$_4$) and Pt$^+$(C$_2$H$_4$) was studied in the visible and near ultra violet by using a dual time-of-flight photofragment spectrometer that has been described in detail previously.[21,22] Metal cations are generated by laser ablation of a translating and rotating rod. To avoid the expense of a solid platinum rod, platinum foil (Sigma-Aldrich, 99.9% pure) was used. The Pt foil (0.0025 in. thick, 1 in. square) was glued to a 0.25 in. o.d. aluminum rod whose central portion was machined down to 0.217 in. o.d. to obtain a relatively smooth, flush surface. For the gold studies, metal ions were obtained by ablation of a 6.1 mm diameter brass rod electroplated with 0.13 mm gold (Fountain Plating, Springfield, MA, 99.97% pure). The resulting ions (Au$^+$ and Pt$^+$) then react with ethylene, or deuterated ethylene (0.3−1% for Au$^+$(C$_2$H$_4$), 4−6% for Pt$^+$(C$_2$H$_4$) and 0.3−1.0% for Au$^+$(C$_2$D$_4$)) seeded in helium introduced through a pulsed valve. Since helium generally

Photofragment Spectroscopy of π Complexes
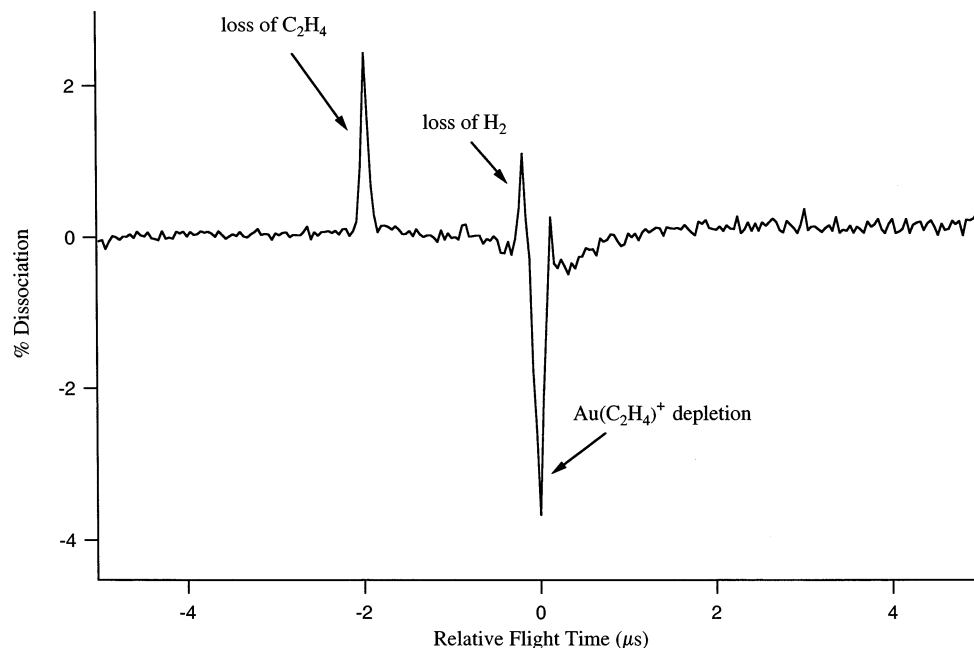
J. Phys. Chem. A, Vol. 108, No. 34, 2004 **6997**

Figure 1. Difference spectrum of $Au(C_2H_4)^+$ at 350 nm. Two channels, loss of H_2 and loss of C_2H_4, are active at this wavelength.

provides poor vibrational cooling, CF_4 (4−6%) was added to the reagent gas mixture to enhance ion cooling.

Ions produced in the source undergo supersonic expansion into vacuum, are skimmed, and then accelerated to 1800 V kinetic energy. Before entering the field-free flight tube the ions are re-referenced to ground potential. The mass-selected cations are then photoexcited at the turning point of the reflectron by the fundamental (laser line width <0.1 cm^{-1}) or frequency-doubled output (laser line width <0.2 cm^{-1}) of a tunable Nd: YAG-pumped dye laser. A dual microchannel plate detector collects the ions and the signal is averaged on a digital oscilloscope. The dissociation channels are determined by their flight times.

Difference spectra were obtained with a home-built chopper wheel, which allows us to identify the dissociation channels present at a specific wavelength by a laser on−laser off technique. Photodissociation spectra were obtained by measuring the fragment ion yield as a function of wavelength and normalizing to the parent ion signal and laser fluence. Ion signals were measured in two ways: by numerically integrating the area under peaks in the difference spectra (for coarse scans), or by using gated integrators to monitor parent and fragment signals.

Results and Discussion

Photofragment spectroscopy can offer valuable thermodynamic and spectroscopic information such as dissociation pathways of the molecule and, from dissociation onsets, upper limits to bond strengths. Photodissociation spectra portray the absorption of ions that dissociate to give the fragment ion being monitored. Above the dissociation limit, the photodissociation spectrum essentially mirrors the absorption spectrum. Furthermore, vibrational structure in the photodissociation spectrum probes the bonding in the excited state.

Photodissociation of $Au^+(C_2H_4)$ and $Pt^+(C_2H_4)$ was monitored from 28 400 to 32 700 cm^{-1} and from 18 400 to 32 500

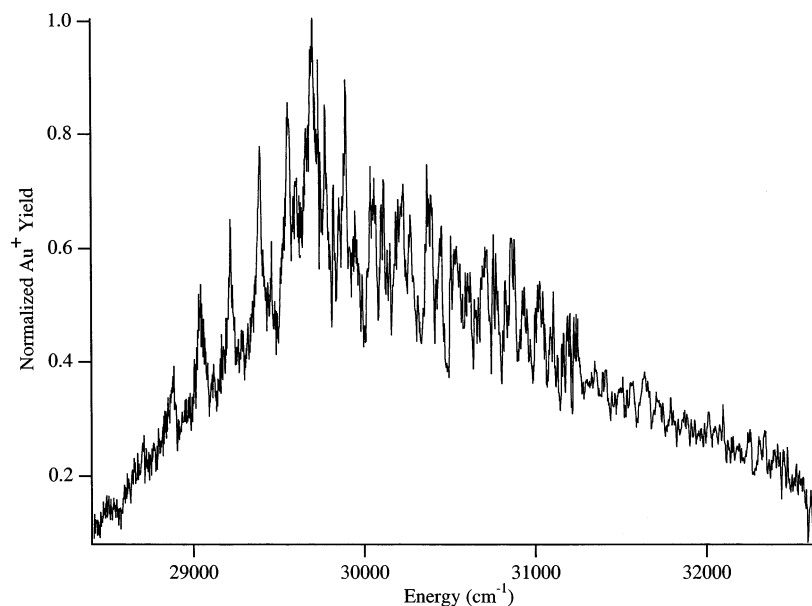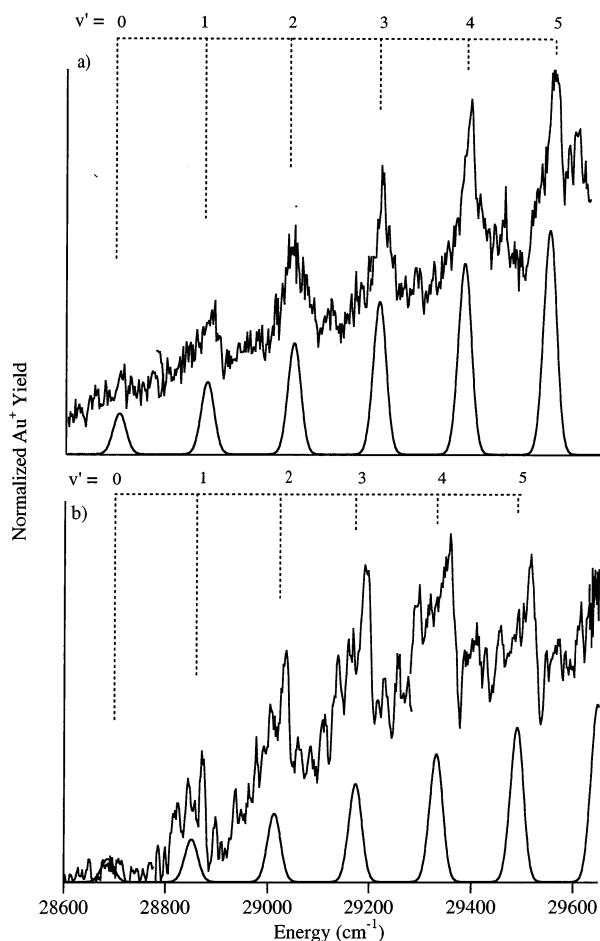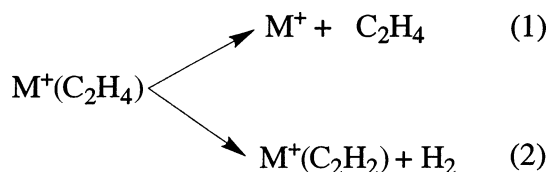**Figure 2.** Photodissociation spectrum of $Au(C_2H_4)^+$.

Figure 3. Enlarged section of the photodissociation spectra of (a) Au-$(C_2H_4)^+$ and (b) Au$(C_2D_4)^+$. The spectra show a progression in the metal−ligand stretch, as indicated by the vibrational numbering and simulated spectra.

cm^{-1} respectively. Difference spectra are ideal for the immediate identification and relative abundance of the dissociation channels that are active at a given wavelength. As shown in Figure 1, the metal−ethylene complexes dissociate through two main channels: loss of ethylene (reaction 1) and loss of hydrogen (reaction 2).

$$M^+(C_2H_4) \Big\langle \begin{array}{l} M^+ + \ C_2H_4 \qquad (1) \\[2em] M^+(C_2H_2) + H_2 \qquad (2) \end{array}$$

However, due to the small difference in masses between the parent and fragment ions, channel (2) could not be monitored accurately and is therefore not discussed in detail. Photodissociation spectra were obtained by monitoring M$^+$ (reaction 1). We observe two large peaks with no resolved vibrational structure in the Pt$^+(C_2H_4)$ dissociation spectrum. On the other hand, for Au$^+(C_2H_4)$ we observe one peak with considerable vibrational structure.

Au$^+$(C$_2$H$_4$): Spectroscopy and Calculations. Scanning the dissociation laser while monitoring the Au$^+$ yield gives rise to the photodissociation spectra shown in Figures 2 and 3. At lower energies, the spectrum consists of a number of well-resolved peaks, reaching a maximum at ∼29 700 cm^{-1}. At higher energies, the spectrum becomes much more congested. This can
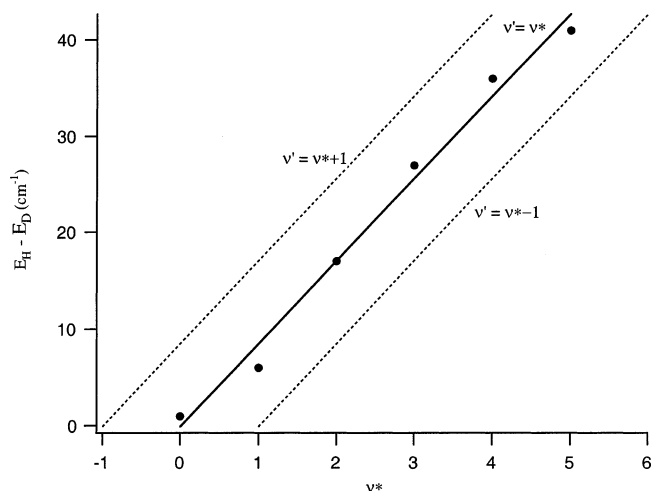

Figure 4. Isotope shift between spectra of Au$(C_2H_4)^+$ and Au$(C_2D_4)^+$ as a function of vibrational numbering. The solid line assumes the peak at 28 870 cm^{-1} corresponds to $\nu' = 1$ (as shown in Figure 3). The upper dashed line assumes it is due to $\nu' = 2$; the lower dashed line assumes it is due to $\nu' = 0$. The isotope shift is given by $E_H - E_D = (1 - \rho)[\omega_H'(\nu' + \frac{1}{2}) - \frac{1}{2}\omega_H'']$, where $\rho = (\mu_H/\mu_D)^{1/2}$ and μ_H and μ_D are the reduced masses of Au$(C_2H_4)^+$ and Au$(C_2D_4)^+$, respectively (refs 23 and 24).

be attributed to a number of factors including contributions from other vibrational modes and possibly from higher lying excited states.

We observe a small amount of photodissociation starting around 28 650 cm^{-1}, and definite dissociation starting at 28 800 cm^{-1}. The higher value provides a conservative upper limit to the Au$^+$−C$_2$H$_4$ bond strength of 344 kJ mol^{-1}. Lack of dissociation can be due to insufficient photon energy or to lack of absorption. As will be shown below, for this system, the dissociation onset is governed by the absorption properties and occurs at energies well above the thermodynamic bond strength.

The low energy portion of the photodissociation spectrum is highlighted in Figure 3. The sequence of peaks spaced by 176 cm^{-1} can be tentatively assigned to a vibrational progression in the metal−ethylene stretch. To confirm this assignment and determine the vibrational numbering we photodissociated the deuterated complex, Au$^+$(C$_2$D$_4$). The vibrational frequency drops to 160 cm^{-1}, as expected based on the higher reduced mass. The vibrational numbering for the metal−ligand stretch is assigned by using the observed energy shifts between analogous peaks in the hydrogenated and deuterated spectra and a pseudodiatomic approach in which the ligand is treated as an atom. This approach has been used by Duncan and co-workers[23] to assign the metal−ligand stretch in Mg$^+$(CO)$_2$. Figure 4 shows a plot of the isotope shift.[24] The solid line shows the assigned vibrational quantum numbering for our experimental data. The two dashed lines show our numbering shifted by one in either direction, justifying the upper state vibrational numbering shown in Figure 3. The adiabatic electronic transition energy (to $\nu' = 0$) is thus 28670 cm^{-1}.

Observation of the H$_2$ loss channel in photodissociation of Au$^+$(C$_2$H$_4$) is interesting, as in the bimolecular reaction of Au$^+$ with ethylene, dehydrogenation

$$Au^+ + C_2H_4 \rightarrow Au^+(C_2H_2) + H_2 \qquad (3)$$

is not observed.[7] This reaction is exothermic by ∼98 kJ mol^{-1} based on the calculated binding energy of Au$^+$ to C$_2$H$_2$ by Frenking and co-workers at the BP86/TZP level[25] and the energetics for the dehydrogenation of ethylene.[26]

TABLE 1: Summary of the Bond Dissociation Energy Calculations for Pt(C₂H₄)⁺ and Au(C₂H₄)⁺ [a]

	SDD basis set (kJ mol⁻¹)			LANL2DZ basis set (kJ mol⁻¹)		
	regular	uncontracted	uncontracted $f = 0.23$	regular	uncontracted	uncontracted $f = 0.23$
$AuC_2H_4^+$	244.0	248.9	252.7	246.0	258.6	261.5
$PtC_2H_4^+$	252.2	255.5	260.7	222.9	228.9	233.6
	(292.5)	(295.8)	(301.0)	(263.2)	(269.2)	(273.9)

[a] For Pt⁺(C₂H₄), the energies listed first include spin−orbit correction whereas those in parentheses correspond to the uncorrected values. All energies are for fully optimized structures and include zero-point energy.

To further investigate the dehydrogenation channel, we photodissociated Au⁺(C₂D₄) at 344 nm (350 kJ mol⁻¹), observing loss of C₂D₄:D₂:D in the ratio 1:0.3:<0.1. Dehydrogenation (reaction 2) is endothermic by ∼208 kJ mol⁻¹.[25,26] Observation of this channel by photodissociation but not in the bimolecular reaction is likely due to more energy being available to overcome exit channel barriers in the photodissociation experiment. Future studies are planned to investigate the loss of D₂ in the deuterated complex.

Schwarz and co-workers have employed both experimental and theoretical techniques to study relativistic effects in the chemistry of the heavier transition metals with a variety of ligands.[15,16,27−30] Most of their studies have concentrated on the coinage metal ions Cu⁺, Ag⁺, and Au⁺. In a combined experimental and computational study with Fourier Transform Ion Cyclotron Resonance (FT-ICR) mass spectrometry, ion bracketing techniques, and ab initio calculations they determined a theoretical bond dissociation energy (BDE) of 305 kJ mol⁻¹ for Au⁺(C₂H₄).[28] In a later study, using ligand exchange reactions (LER) they obtained a lower limit for the BDE of 247 kJ mol⁻¹.[16] Both of these values are consistent with our upper limit of 344 kJ mol⁻¹. Investigations into the bonding of Cu⁺, Ag⁺, and Au⁺ with ethylene were performed by Hertwig et al.[30] They predicted that in all three metals covalency accounts for 40% of the bonding, with the remainder assigned to electrostatic factors. For the Cu⁺ complex, BDE = 214 kJ mol⁻¹, π bonding accounts for about one-third of the total covalent contribution and about one-fifth for Ag⁺(C₂H₄) and Au⁺(C₂H₄) whose BDE's are calculated to be 154 and 287 kJ mol⁻¹, respectively. This contrasts with the much earlier work of Ziegler,[31] who predicted that σ donation contributes equally to all three complexes but π back-donation is important only for Cu(C₂H₄)⁺. Hertwig et al. conclude that the Cu⁺(C₂H₄) and Au⁺(C₂H₄) complexes are cyclic whereas the Ag⁺(C₂H₄) complex is T-shaped.[30] These studies imply that complexes with high bond energies should adopt the metallocyclopropane structure whereas weaker binding complexes should be T-shaped.

Since there are no calculations on the dissociation energy of Pt(C₂H₄)⁺ we decided to perform calculations on this system as well as Au⁺(C₂H₄). These calculations provide geometries of the complexes, vibrational frequencies, and thermodynamic information such as bond dissociation energies. Bond dissociation energies for Au⁺(C₂H₄) and Pt⁺(C₂H₄) were determined with use of the B3LYP hybrid density functional theory (DFT) via the Gaussian 98 program.[32] In addition, we calculated potentials along the metal−ligand stretch for several excited electronic states using time-dependent DFT (TD-DFT). We performed a number of calculations at the B3LYP level using several modifications of the SDD and LANL2DZ relativistic effective core potentials and basis sets for the metals and the 6-311+G(d,p) basis set for C and H. These calculations do not explicitly include spin−orbit effects, which should not be important for the gold complex as Au⁺ and Au⁺(C₂H₄) have

singlet ground states. The effect of basis set superposition error (BSSE) on bond strengths was estimated by using the counterpoise method. As the error was found to be <1 kJ mol⁻¹ it was not included. All calculations include geometry optimization and a frequency calculation for each basis set.

Because we found that the computed binding energy depends on the basis set, binding energies were calculated by using both uncontracted and contracted SDD ([8s/7p/6d]/[6s/5p/3d]) and LANL2DZ ([8s/6p/3d]/[3s/3p/2d]) basis sets for gold. For the SDD basis, the uncontraction had minimal effect on the binding energy, increasing the BDE only slightly from 244 kJ mol⁻¹ to 249 kJ mol⁻¹. However, for the LANL basis set there was a slightly larger increase from 246 kJ mol⁻¹ to 259 kJ mol⁻¹. Table 1 summarizes our results. Adding a set of f-polarization functions ($\zeta = 0.23$) to the uncontracted basis sets increased the bond strengths to 253 (SDD) and 262 kJ mol⁻¹ (LANL), but these values are still considerably lower than those previously obtained by Hertwig et al. and Schröder et al., 287 kJ and 305 kJ mol⁻¹,[16,30] and by Frenking and co-workers, also 305 kJ mol⁻¹.[25] All of these values are consistent with experimental data, which gives a broad range: 247 kJ mol⁻¹ ≤ BDE ≤ 344 kJ mol⁻¹. Guided ion beam measurements[33] of the Au⁺−ethylene bond strength could greatly reduce the uncertainty in the experimental value.

One possible explanation for the differences between our computed binding energies and those of Hertwig et al. and Schröder et al.[29,30] is the larger, more flexible basis sets that they used. The addition of two diffuse d functions as well as an extra f function resulted in a [10s/8p/7d/1f]/(9s/5p/6d/1f) contraction for gold and the augmentation of the Dunning TZ2P basis for carbon by an f function gave a [10s/6p/2d/1f]/(5s/3p/2d/1f) contraction. Interestingly, for Au⁺(CO), using the SDD basis set for Au and 6-311+G(d,p) for C and O, we obtain the same bond strength (182 kJ mol⁻¹) as Hertwig et al.[34] Our calculations suggest that a very large, flexible basis set is required to reproduce bond strengths for side-on complexes such as M⁺(C₂H₄) accurately. The bonding in linear complexes such as Au⁺(CO) is much simpler and smaller basis sets are sufficient.

The application of DFT calculations has revolutionized the understanding of the ground electronic states of transition metal complexes,[35−37] and the development of time-dependent DFT (TD-DFT) allows the efficient calculation of excited electronic states and the electronic transition intensities in molecules. TD-DFT calculations have predominantly been employed for closed shell organic[38,39] and inorganic[40,41] compounds. However, TD-DFT calculations on open-shell systems containing transition metals show good agreement with experimental results.[42−44] The low cost and simplicity of TD-DFT calculations make it an especially useful tool when combining experimental with theoretical studies.

Additional calculations with the TD-DFT methodology were carried out to complement our experimental findings and to further confirm our assignment of the vibrational progression. Calculations of excited states that are formed by the promotion
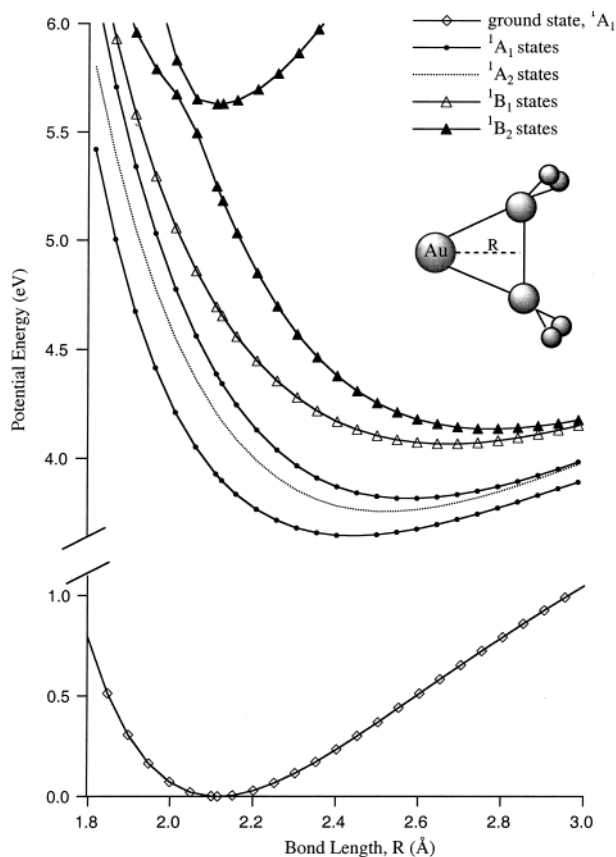
Figure 5. Adiabatic potential energy curves along the metal–ligand stretch of the ground and low-lying singlet states of $Au(C_2H_4)^+$, from TD-DFT calculations. R is the distance between the Au^+ atom and the midpoint of the C–C bond.

TABLE 2: Bond Lengths (Å) and Bond Angles (degrees) of the Optimized Geometries for $Pt(C_2H_4)^+$, $Au(C_2H_4)^+$, and Related Molecules[a]

	C–C	M^+-C	HCH	HCC	HCCH (pyramidalization)
C_2H_6	1.530		107.5	111.4	
C_2H_4	1.329		116.5	121.7	180
					(0)
C_2H_4O	1.467	1.450	115.7	119.6	153.5
					(26.5)
$Au^+(C_2H_4)$	1.397	2.227	117.0	120.6	164.7
					(15.3)
$Pt^+(C_2H_4)$	1.415	2.137	116.4	120.3	159.9
					(20.1)

[a] Calculations performed at the B3LYP level, using the SDD basis set for Au and Pt and the 6-311G+(d,p) basis set for C, H, and O. The pyramidalization angle is 180° − (HCCH dihedral angle).
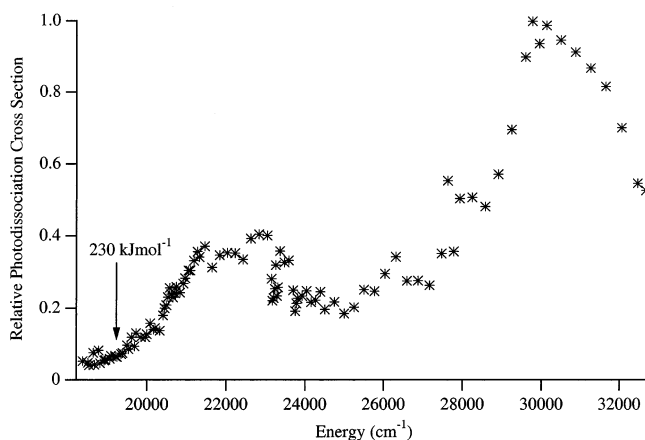

Figure 6. Photodissociation spectrum of $Pt(C_2H_4)^+ + h\nu \rightarrow Pt^+ + C_2H_4$. The Pt^+ photosignal is a sum of the three main isotopes ([194]Pt, [195]Pt, and [196]Pt) and is normalized to the parent ion signal and laser power. A relative cross section of 1 corresponds to $\sigma \approx 5 \times 10^{-19}$ cm^2.

of one electron from the ground state, conserving spin, lead to the potential energy curves shown in Figure 5. These are adiabatic potentials: promotion energies are calculated from optimized geometries at each value of the metal–ligand bond length, R. The calculations for $Au^+(C_2H_4)$ were performed at the B3LYP level, using the SDD basis set for Au and 6-311+G-(d,p) for C and H. The first excited state shown ($^1A_1$) is at a vertical energy of 3.9 eV (31460 cm^{-1}) and has the highest calculated oscillator strength ($f = 0.0321$) of the states shown.

Using the calculated potentials for the ground and first excited state, we numerically solve the one-dimensional Schrödinger equation for the metal–ligand stretch vibration. We then simulate the vibrational structure in the photodissociation spectra of $Au^+(C_2H_4)$ and $Au^+(C_2D_4)$ by calculating the Franck–Condon factors for transitions from the ground ($v'' = 0$) vibrational state. The simulated spectra are shown in Figure 3. The only adjustable parameter is the absolute excitation energy, which is shifted by 1490 cm^{-1} to lower energy from the calculated value. The calculated vibrational frequencies are in excellent agreement with experiment. The calculations also predict that the metal–ligand bond length (denoted by R in Figure 5) increases from 2.12 to 2.45 Å upon electronic excitation. As a result, the excited state exhibits a lower metal–ligand stretch frequency than that of the ground state (321 cm^{-1}). The peaks in the photodissociation spectrum are quite wide, ~50 cm^{-1} (fwhm), and have a vibrational frequency of 176 cm^{-1}, with no obvious anharmonicity. The widths give a lower limit to the predissociation lifetime of ~100 fs. The simulation predicts a vibrational frequency of 183 cm^{-1} and an anharmonicity of 1 cm^{-1}. The small anharmonicity is likely because the vibrations sampled are deep in the potential well.

The TD-DFT calculations suggest that our 28 800 cm^{-1} (344 kJ mol^{-1}) onset to dissociation is due to lack of absorption at lower energies, rather than to having insufficient energy to break the metal–ligand bond. We observe transitions to $v' = 1$ of the lowest excited singlet state, at 28 800 cm^{-1}, and may observe transitions to $v' = 0$ at 28 670 cm^{-1}. However, we do not observe dissociation at lower energies simply because there are no excited singlet electronic states below this energy. The small number of excited electronic states is due to the $5d^{10}6s^0$ electronic configuration of Au^+. The increased complexity of the spectrum as we move to higher energy could be due to transitions to higher lying electronic states or to progressions in other vibrations.

In addition to the thermodynamic and spectroscopic studies we also investigated the geometries of both $Au^+(C_2H_4)$ and Pt^+-(C_2H_4). Our calculations for $Au^+(C_2H_4)$ are consistent with those of Hertwig et al.,[30] who concluded via an atoms-in-molecule (AIM) analysis that this complex adopts the metallocyclopropane structure. The details of this analysis are summarized in Table 2 and will be discussed in more detail below.

$Pt^+(C_2H_4)$: Spectroscopy and Calculations. Pt^+ has the electronic configuration $5d^96s^0$ and, unlike Au^+, has the added complication of spin–orbit coupling. The photodissociation spectrum (Figure 6) was obtained via difference spectra where dissociation of ions containing the three main isotopes of platinum, i.e., [194]Pt^+, [195]Pt^+, and [196]Pt^+, were monitored and summed. As seen in the figure, the spectrum shows two maxima, a more intense peak at 30 300 cm^{-1} and a less intense peak at

Photofragment Spectroscopy of π Complexes

J. Phys. Chem. A, Vol. 108, No. 34, 2004 **7001**

21 600 cm^{-1}. At the lower energy end of the spectrum we can extrapolate to obtain an approximate onset to dissociation of 19 200 cm^{-1}, which in turn gives an upper limit to the bond strength of 230 kJ mol^{-1}. Photodissociation persists to lower energy but with extremely low yield.

In parallel with the gold studies, we scanned the laser using smaller steps in search of vibrational structure but none was observed. The lack of vibrational structure is most likely due to a combination of rapid, direct dissociation and rapid photo-induced reactions. While there have been several studies of Au$^+$(C$_2$H$_4$),[15,16,25,27−30,45−47] there is very little data available for the platinum species. Theoretical studies by Schröder et al. on PtCH$_2^+$ and [H−Pt−CH$_3$]$^+$ complexes have yielded estimates for BDE(Pt$^+$−C$_2$H$_4$) ≈ 230 kJ mol^{-1}.[15,16] This value is, coincidentally, identical with our experimental upper limit and is considerably lower than that of the gold system. To complement our experimental results on Pt$^+$(C$_2$H$_4$) we performed B3LYP calculations. Since the calculations do not explicitly include spin−orbit coupling, there is an ambiguity in the calculation of bond dissociation energies, as spin−orbit effects are larger in Pt$^+$ than in Pt$^+$(C$_2$H$_4$). One method is to calculate dissociation energies as for closed shell species, essentially assuming that spin−orbit effects stabilize Pt$^+$ and Pt$^+$(C$_2$H$_4$) equally.[48] The second limiting approach is to correct the dissociation energy by the *J*-weighted average spin−orbit energies of the Pt$^+$ ground state, 40.3 kJ mol^{-1}. This assumes no spin−orbit stabilization of the complex, and thus likely overestimates the true spin−orbit correction.[49−51] We calculated the Pt$^+$−C$_2$H$_4$ bond dissociation energy using the same basis sets as for Au$^+$(C$_2$H$_4$). The results are summarized in Table 2. Spin−orbit corrected results are shown first; uncorrected results are shown below in parentheses. Calculations with the SDD basis set show a pattern similar to those of the Au$^+$(C$_2$H$_4$) system, with uncontraction and addition of an f function increasing the bond strength by ∼9 kJ mol^{-1}. However, unlike gold, calculations with the smaller LANL basis set give significantly lower bond strengths. Our calculations predict a bond strength for Pt$^+$(C$_2$H$_4$) of ∼260 kJ mol^{-1}. This is slightly too high, as it lies 30 kJ mol^{-1} above the upper limit obtained from our experimental results.

To characterize the excited states of Pt$^+$(C$_2$H$_4$) we performed TD-DFT calculations (SDD basis set for Pt and 6-311+G(d,p) for C and H). The resulting adiabatic potentials along the Pt$^+$−ethylene stretch are illustrated in Figure 7. Clearly, Pt$^+$(C$_2$H$_4$) has many low-lying excited electronic states, especially when compared to Au$^+$(C$_2$H$_4$). These excited electronic states are likely to mix once spin−orbit coupling is introduced. Transitions to most of the states shown are predicted to be very weak. The most intense transitions are to the 7th state ($^1A_1$, f = 0.0028) at a vertical energy of 3.36 eV (27 100 cm^{-1}), the 11th state ($^1A_1$, f = 0.0142) at a vertical energy of 3.97 eV (32 060 cm^{-1}), and the 14th state ($^1B_1$, f = 0.0065) at a vertical energy of 4.32 eV (34 850 cm^{-1}). All other excited states shown have minimal if any oscillator strength. For comparison, the photodissociation spectrum consists of two main peaks at ∼21 600 and 30 300 cm^{-1} and possibly a third minor peak at 26 500 cm^{-1}. The agreement between the experimental and calculated excitation energies is significantly poorer for Pt$^+$(C$_2$H$_4$) than for Au$^+$(C$_2$H$_4$). This is probably due to the omission of spin−orbit coupling in the calculation. Spin−orbit coupling should be substantial for Pt$^+$(C$_2$H$_4$). For example, Rakowitz et al.[52] have explicitly calculated the effect of spin−orbit coupling on several excited states of PtCH$_2^+$ and find transition energies to shift by ∼1000−3000 cm^{-1}.
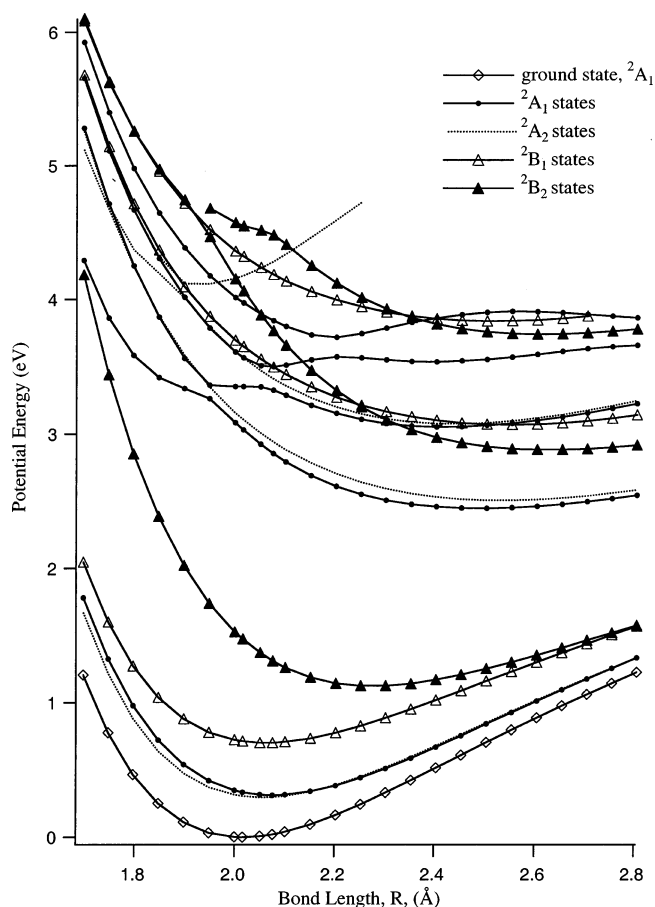

Figure 7. Adiabatic potential energy curves along the metal−ligand stretch of the ground and low-lying doublet states of Pt(C$_2$H$_4$)$^+$. *R* is the distance between the Pt$^+$ atom and the midpoint of the C−C bond, as in Figure 5.

We also investigated the geometries of our complexes. In an atoms-in-molecules[53] (AIM) analysis, Hertwig et al.[30] predict a more electrostatic binding for Cu$^+$ and Ag$^+$ analogues (BDE's of 181 and 141 kJ mol^{-1}, respectively) and T-shape structures. However, for Au$^+$(C$_2$H$_4$) the AIM analysis clearly shows there are bond critical points between the gold and the carbon atoms, implying more covalency in the bonding, and a cyclic structure. If we look more closely at the geometry of Au$^+$(C$_2$H$_4$) we see that as the gold atom nears the ethylene, the C−C bond elongates by 0.068 Å from that of the free ethylene (Table 2). In the Dewar−Chatt−Duncanson model this is attributed to an increase in σ-acceptor and π-donor contributions from the metal, which moves electron density from the π bonding orbital to the π* antibonding orbital in the ethylene. Hertwig et al. also discuss the effect of rehybridization of the carbon centers from sp^2 to sp^3, which results in a partial pyramidalization of the carbon centers. In essence, the greater the covalent interaction of the M$^+$ with ethylene, the greater the pyramidalization, and most of all, elongation of the C−C bond, resulting in more sp^3 bonding and hence a more cyclic geometry.

Since Au$^+$(C$_2$H$_4$) has already been assigned the metallocyclopropane structure we can compare the bond lengths and angles in Au$^+$(C$_2$H$_4$) to those of Pt$^+$(C$_2$H$_4$) and ethylene oxide, a known cyclic structure. This will enable us to assign the appropriate geometry for Pt$^+$(C$_2$H$_4$). A summary of our results is shown in Table 2. As stated previously, the level of pyramidalization and degree of elongation of the C−C bond are strong indications of the extent of covalent interaction of the M$^+$ with ethylene. The C−C bond in Pt$^+$(C$_2$H$_4$) (1.415 Å)

Stringer et al.

is longer than that in Au$^+$(C$_2$H$_4$) (1.397 Å) and closer to that of the known cyclic compound, C$_2$H$_4$O (1.467 Å). Furthermore, the level of pyramidalization is also greater in Pt$^+$(C$_2$H$_4$) than in Au$^+$(C$_2$H$_4$), and again, closer to that observed in ethylene oxide. We can therefore assign a metallocyclopropane conformation to the Pt$^+$(C$_2$H$_4$) complex. The lower bond strength in Pt$^+$(C$_2$H$_4$) relative to Au$^+$(C$_2$H$_4$) is thus likely due to spin−orbit coupling stabilizing Pt$^+$ much more than Pt$^+$(C$_2$H$_4$).

Summary and Conclusions

Photodissociation spectra are reported for Pt$^+$(C$_2$H$_4$) and Au$^+$-(C$_2$H$_4$). The Pt$^+$(C$_2$H$_4$) spectrum, studied between 18 400 and 32 500 cm^{-1}, shows two broad peaks at 21 600 and 30 300 cm^{-1}. The dissociation onset of 19 200 cm^{-1} provides an upper limit to the bond strength of 230 kJ mol^{-1}. Photodissociation of Au$^+$(C$_2$H$_4$) between 28 400 and 32 700 cm^{-1} yields one band with extensive vibrational structure, prominently featuring a 176-cm^{-1} progression. With the aid of the spectrum of Au$^+$(C$_2$D$_4$), we assign this vibrational progression to the metal−ligand stretch and obtain an adiabatic electronic transition energy of 28 670 cm^{-1}. The onset to photodissociation of 28 800 cm^{-1} gives an upper limit to the bond strength of 344 kJ mol^{-1}.

DFT calculations have provided valuable information on the binding energies and geometries of the two complexes. Bond dissociation energies depend on the basis set used, varying from 246 to 262 kJ mol^{-1} for Au$^+$(C$_2$H$_4$) and 223 to 261 kJ mol^{-1} for Pt$^+$(C$_2$H$_4$) These results are consistent with our experimental findings. In addition, comparisons of the bond lengths and angles in Pt$^+$(C$_2$H$_4$) to those of Au$^+$(C$_2$H$_4$) and ethylene oxide, a known cyclic compound, leads us to predict that Pt$^+$(C$_2$H$_4$) exhibits more covalent character than electrostatic and therefore adopts a metallocyclopropane structure.

References and Notes

(1) Zeise, W. C. *Pogg. Ann. Phys.* **1827**, *9*, 632.

(2) Zeise, W. C. *Pogg. Ann. Phys.* **1831**, *21*, 497−541. English translation and historical introduction in: Kauffman, G. B. *Classics in Coordination Chemistry*; Dover: New York, 1976; Vol. 2, pp 17−37.

(3) Crabtree, R. H. *The Organometallic Chemistry of the Transition Metals*, 2nd ed.; John Wiley & Sons Inc: New York, 1994.

(4) Dewar, M. J. S.; Ford, G. P. *J. Am. Chem. Soc.* **1979**, *101*, 783−791.

(5) Michael, D.; Mingos, P. *J. Organomet. Chem.* **2001**, *635*, 1−8.

(6) Weil, D. A.; Wilkins, C. L. *J. Am. Chem. Soc.* **1985**, *107*, 7316−7320.

(7) Chowdhury, A. K.; Wilkins, C. L. *J. Am. Chem. Soc.* **1987**, *109*, 5336−5343.

(8) Hettich, R. L.; Jackson, T. C.; Stanko, E. M.; Freiser, B. S. *J. Am. Chem. Soc.* **1986**, *108*, 5086−5093.

(9) Ranasinghe, Y. A.; MacMahon, T. J.; Freiser, B. S. *J. Am. Chem. Soc.* **1992**, *114*, 9112.

(10) Lu, W.-Y.; Kleiber, P. D.; Young, M. A.; Yang, K.-H. *J. Chem. Phys.* **2001**, *115*, 5823−5829.

(11) Pyykkö, P. *Chem. Rev.* **1988**, *88*, 563−594.

(12) Viellard, A. *Chem. Rev.* **1991**, *91*, 743−766.

(13) Sodupe, M.; Bauschlicher, C. W., Jr. *J. Phys. Chem.* **1991**, *95*, 8640−8645.

(14) Sodupe, M.; Bauschlicher, C. W., Jr.; Langhoff, S. R.; Partridge, H. *J. Phys. Chem.* **1992**, *96*, 2118−2122.

(15) Schröder, D.; Diefenbach, M.; Schwarz, H. In *Relativistic Effects in Heavy Element Chemistry and Physics*; Hess, B. A., Ed.; John Wiley & Sons Ltd.: Chichester, UK, 2003; pp 245−258.

(16) Schröder, D.; Schwarz, H.; Hrusák, J.; Pyykkö, P. *Inorg. Chem.* **1998**, *37*, 624−632.

(17) Freiser, B. S. *Organometallic Ion Chemistry*; Kluwer Academic Publishers: Dordrecht, The Netherlands, 1996.

(18) Metz, R. B. *Int. Rev. Phys. Chem.* **2004**, *23*, 79−108.

(19) Ervin, K. M. *Chem. Rev.* **2001**, *101*, 391.

(20) Duncan, M. A. *Int. Rev. Phys. Chem.* **2003**, *22*, 407−435.

(21) Husband, J.; Aguirre, F.; Ferguson, P.; Metz, R. B. *J. Chem. Phys.* **1999**, *111*, 1433−1437.

(22) Aguirre, F.; Husband, J.; Thompson, C. J.; Metz, R. B. *Chem. Phys. Lett.* **2000**, *318*, 466−470.

(23) Yeh, C. S.; Willey, K. F.; Robbins, D. L.; Pilgrim, J. S.; Duncan, M. A. *J. Chem. Phys.* **1993**, *98*, 1867−1875.

(24) Herzberg, G. *Molecular Spectra and Molecular Structure. I. Spectra of Diatomic Molecules*; Van Nostrand Reinhold Company: New York, 1950.

(25) Nechaev, M. S.; Rayón, V. M.; Frenking, G. *J. Phys. Chem. A* **2004**, *108*, 3134−3142.

(26) Linstrom, P. J.; Mallard, W. G. *NIST Chemistry WebBook, NIST Standard Database Number 69*; National Institute of Standards and Technology: Gaithersburg, MD, 2003 (http://webbook.nist.gov).

(27) Schwarz, H. *Angew. Chem., Int. Ed.* **2003**, *42*, 4442−4454.

(28) Schröder, D.; Hrusák, J.; Hertwig, R. H.; Koch, W.; Schwerdtfeger, P.; Schwarz, H. *Organometallics* **1995**, *14*, 312−316.

(29) Schröder, D.; Wesendrup, R.; Hertwig, R. H.; Dargel, T. K.; Grauel, H.; Koch, W.; Bender, B. R.; Schwarz, H. *Organometallics* **2000**, *19*, 2608−2615.

(30) Hertwig, R. H.; Koch, W.; Schröder, D.; Schwarz, H.; Hrusák, J.; Schwerdtfeger, P. *J. Phys. Chem.* **1996**, *100*, 12253−12260.

(31) Ziegler, T.; Rauk, A. *Inorg. Chem.* **1979**, *18*, 1558−1565.

(32) Frisch, M. J.; Trucks, G. W.; Schlegel, H. B.; Scuseria, G. E.; Robb, M. A.; Cheeseman, J. R.; Zakrzewski, V. G.; Montgomery, J. A.; Stratmann, R. E.; Burant, J. C.; Dapprich, S.; Millam, J. M.; Daniels, A. D.; Kudin, K. N.; Strain, M. C.; Farkas, O.; Tomasi, J.; Barone, V.; Cossi, M.; Cammi, R.; Mennucci, B.; Pomelli, C.; Adamo, C.; Clifford, S.; Ochterski, J.; Petersson, G. A.; Ayala, P. Y.; Cui, Q.; Morokuma, K.; Malick, D. K.; Rabuck, A. D.; Raghavachari, K.; Foresman, J. B.; Cioslowski, J.; Ortiz, J. V.; Stefanov, B. B.; Liu, G.; Liashenko, A.; Piskorz, P.; Komaromi, I.; Gomperts, R.; Martin, R. L.; Fox, D. J.; Keith, T.; Al-Laham, M. A.; Peng, C. Y.; Nanayakkara, A.; Gonzalez, C.; Challacombe, M.; Gill, P. M. W.; Johnson, B. G.; Chen, W.; Wong, M. W.; Andres, J. L.; Head-Gordon, M.; Replogle, E. S.; Pople, J. A. *Gaussian 98*, Revision A.3; Gaussian, Inc.: Pittsburgh, PA, 1998.

(33) Armentrout, P. B. *Int. J. Mass Spectrom.* **2003**, *227*, 289−302.

(34) Hertwig, R. H.; Hrusák, J.; Schröder, D.; Koch, W.; Schwarz, H. *Chem. Phys. Lett.* **1995**, *236*, 194−200.

(35) Yoshizawa, K.; Shiota, Y.; Yamabe, T. *J. Chem. Phys.* **1999**, *111*, 538−545.

(36) Glukhovtsev, M. N.; Bach, R. D.; Nagel, C. J. *J. Phys. Chem. A* **1997**, *101*, 316−323.

(37) Thompson, C. J.; Aguirre, F.; Husband, J.; Metz, R. B. *J. Phys. Chem. A* **2000**, *104*, 9901−9905.

(38) Matsuzawa, N. N.; Ishitani, A.; Dixon, D. A.; Uda, T. *J. Phys. Chem. A* **2001**, *105*, 4953.

(39) Wiberg, K. B.; Stratmann, R. E.; Frisch, M. J. *Chem. Phys. Lett.* **1998**, *297*, 60.

(40) Farrell, I. R.; van Slageren, J.; Zalis, S.; Vlcek, A. *Inorg. Chim. Acta* **2001**, *315*, 44.

(41) van Gisbergen, S. J.; Groeneveld, J. A.; Rosa, A.; Snijders, J. G.; Baerends, E. J. *J. Phys. Chem. A* **1999**, *103*, 6835.

(42) Borowski, T.; Broclawik, E. *Chem. Phys. Lett.* **2001**, *339*, 433.

(43) Broclawik, E.; Piskorz, W.; Adamska, K. *J. Chem. Phys.* **1999**, *110*, 11685−11687.

(44) Aguirre, F.; Husband, J.; Thompson, C. J.; Stringer, K. L.; Metz, R. B. *J. Chem. Phys.* **2002**, *116*, 4071−4078.

(45) Uddin, J.; Dapprich, S.; Frenking, G. *Organometallics* **1999**, *18*, 457−465.

(46) Pidun, U.; Frenking, G. *J. Organomet. Chem.* **1996**, *525*, 269−278.

(47) Massera, C.; Frenking, G. *Organometallics* **2003**, *22*, 2758−2765.

(48) Thompson, C. J.; Stringer, K. L.; McWilliams, M.; Metz, R. B. *Chem. Phys. Lett.* **2003**, *376*, 588−594.

(49) Zhang, X.-G.; Liyanage, R.; Armentrout, P. B. *J. Am. Chem. Soc.* **2001**, *123*, 5563−5575.

(50) Zhang, X.-G.; Armentrout, P. B. *J. Chem. Phys.* **2002**, *116*, 5565−5573.

(51) Zhang, X.-G.; Armentrout, P. B. *J. Phys. Chem. A* **2003**, *107*, 8904−8914.

(52) Rakowitz, F.; Marian, C. M.; Schimmelpfennig, B. *Phys. Chem. Chem. Phys.* **2000**, *2*, 2481−2488.

(53) Bader, R. F. W. *The International Series of Monographs on Chemistry. No. 22: Atoms in Molecules−A Quantum Theory*; Oxford University Press: New York, 1990.